Biosensors and Bioelectronics 53 (2014) 340–345

Contents lists available at ScienceDirect

Biosensors and Bioelectronics

journal homepage: www.elsevier.com/locate/bios

An aptamer-based biosensor for sensitive thrombin detection with phthalocyanine@SiO_2 mesoporous nanoparticles

Zhou Jiang [b,c], Tingting Yang [b,c], Minyan Liu [a,c], Yanli Hu [a,c], Jian Wang [a,c,*]

[a] Ministry of Education Key Laboratory of Analysis and Detection for Food Safety, Fujian Provincial Key Laboratory of Analysis and Detection for Food Safety, Fuzhou University, Fuzhou 350108, China
[b] Institute of Research on Functional Materials, Cancer Metastasis Alert and Prevention Center, Fuzhou University, Fuzhou 350108, China
[c] College of Chemistry and Chemical Engineering, Fuzhou University, Fuzhou 350108, China

ARTICLE INFO

Article history:
Received 29 June 2013
Received in revised form
28 September 2013
Accepted 3 October 2013
Available online 16 October 2013

Keywords:
Tetra-α-(24-di-tert-butylphenoxy)-phthalocyaninato zinc
Silica nanoparticle
Thrombin
Chemiluminescence

ABSTRACT

Silica nanoparticles, with entrapped hydrophobic photosensitizer tetra-α-(2, 4-di-tert-butylphenoxy)-phthalocyaninato zinc ($ZnPc(OAr)_4$), were synthesized by hydrolyzing triethoxyvinylsilane (TEVS) and 3-amino propyl triethoxysilane (APTES). The as-prepared nanoparticles, which were highly monodispersed spheres (about 100 nm), exhibited strong Q-band absorption of $ZnPc(OAr)_4$ centered at 701 nm. The aqueous solubility of ZnPc(OAr)4 encapsulated in silica nanoparticles was obviously improved. The nanoparticles efficiently generated singlet oxygen ($^1O_2$) both in organic and aqueous solutions after being irradiated at suitable wavelength. The resulting $^1O_2$ then initiated chemiluminescence (CL) by reacting with a methyl cypridina luciferin analog (MCLA). Based on the photoinduced CL, a sensitive aptamer-based sandwich-type sensor was presented to detect human thrombin. Thrombin was first attached to $Pc@SiO_2$ via secondary aptamer, and then they were collected, for CL determination, by beads with primary aptamer. The proposed approach, which was highly selective with a low detection limit of 80 pmol/L, minimized the nonspecific adsorption. Such an aptamer-based biosensor is feasible in screening biomarkers in complex matrices at ultratrace levels.

1. Introduction

Photodynamic therapy (PDT), as one of the important therapeutic options in the management of cancer and other diseases, has attracted extensive attentions recently by treating various tumors with triumphs (Triesscheijn et al., 2006; Dolmans et al., 2003; Huang, 2005). This method is based on the preferential localization of light-sensitive species or photosensitizers (PSs) in target tissues upon systemic administration. When such PSs are irradiated with visible or near-infrared (NIR) light at appropriate wavelength, the excited molecules can transfer energy to surrounding molecular oxygen normally in its triplet ground state, forming reactive oxygen species (ROS) such as singlet oxygen ($^1O_2$) or free radicals.

Phthalocyanine (Pc) and its substituted derivatives (Pcs), which absorb intensely at 600–900 nm (Q-band), the useful therapeutic window region of PDT due to potent tissue penetration (Leznoff, 1989, 1993, 1996), have been extensively studied as the second-generation PSs. However, phthalocyanines commonly suffer from hydrophobicity and aggregation (especially in aqueous solutions) owing to large π-conjugated systems which reduce the photosensitizing efficiency. Although many water-soluble Pcs have been synthesized by introducing hydrophilic moieties, such as carboxylate, sulfonate, glucose, phosphonate, polyoxyethylene, amino and carboxyl groups, most of them are highly aggregated in water.

Numerous researchers have used nanomaterials as drug carriers for PDT (Bechet et al., 2008; Wang et al., 2004; Sadzuka et al., 2007; Roy et al., 2003; Tang et al., 2005), of which silica particles can be easily prepared with desired size, shape, porosity, and remarkable stability. Therefore, silica-based nanoparticles may not release encapsulated drugs with changing pH and temperature, and can also effectively protect embedded molecules (enzymes, drugs, etc.) against denaturation induced by external environment. Meanwhile, silica is known for its biocompatibility and ease of modifying surfaces with a variety of functional groups using silane chemistry and commercially available biotargeting organic silicon reagents (Rossi et al., 2005; Kim et al., 2009; Zhu et al., 2011). Silica nanoparticles have been widely applied in nanobiotechnology as drug carriers. For example, Yan and Kopelman (2003) encapsulated phthalocyanine silicon, a hydrophobic second-generation PS, in ca. 37 nm silica spheres. The dosage of PS delivered to cancer cells was increased by approximately two orders of magnitude with over fourfold increase in the PDT efficiency. In this study, we focused on the synthesis of PS-doped silica-based nanoparticles by appropriately

* Corresponding author. Tel.: +86 131 594 04006.
E-mail address: jwang@fzu.edu.cn (J. Wang).

0956-5663/$ - see front matter © 2013 Elsevier B.V. All rights reserved.
http://dx.doi.org/10.1016/j.bios.2013.10.005

controlling the ratio of raw material in micellar media. The as-prepared nanoparticles may be both soluble and non-aggregated in aqueous solutions and cater to the requirements of PDT by efficient $^1O_2$ generation.

Thrombin, a kind of serine protease, plays an important role in coagulation cascade, thrombosis and hemostasis. The protein, even at picomolar range in blood, is associated with diseases, thus requiring highly sensitive analytical protocols. Inspired by previous literatures (Cho et al., 2008; Niu et al., 2013; Xu et al., 2013), we aimed to develop a selective and sensitive aptamer-based sandwich-type sensor to detect thrombin in human serum. This method is sensitive, selective, and is especially suitable for detecting proteins in real samples with moderate consumption.

2. Experimental section

2.1. Reagent and chemicals

Thrombin and 2-mercaptoethanol were purchased from Sigma-Aldrich (USA). Aptamers were purchased from Sangon (Shanghai). Their sequences are as follows: the primary aptamer 50-SH-$(CH_2)_6$-TT TTTTT TTG GTT GGT GTG GTT GG-30 and the secondary aptamer 50-biotin-GGT TGG TGT GGT TGG-30 (Bock et al., 1992; Yang et al., 2009). All chemicals were of analytical grade and were used without further purification. All solutions were prepared with bidistilled water.

Tetra-α-(2,4-di-tert-butylphenoxy)-phthalocyaninato zinc (ZnPc$(OAr)_4$) and tetra-β-(potassium sulfonate) phthalocyaninato zinc ($ZnPcS_4$) were synthesized in our lab as previously described (Xu et al., 2011; Jiang et al., 2005; Ogunsipe and Nyokong, 2005). Nonsubstituted phthalocyaninato zinc (ZnPc) was purchased from Sigma-Aldrich. Their chemical structures are shown in Fig. 1.

Tween-80, N,N-dimethyl formamide (DMF), ethanol, n-butanol, and ammonia solution (25–28%) were purchased from Sinopharm Chemical Reagent Co., Ltd., China. Triethoxyvinylsilane (TEVS), 3-aminopropyl-triethoxysilane (APTES), and 2-methyl-6-(4-methoxyphenyl)-3,7-dihydronimid (MCLA) were purchased from Sigma-Aldrich and used without any further purification. All photophysical experiments were carried out using analytical grade solvents. Distilled water prepared by our lab was used throughout the experiments.

2.2. Method for encapsulating PSs in SiO_2 nanoparticles

In brief, the nanoparticles were synthesized using the microemulsion method. Tween-80 (0.2 g) was dissolved in 10 mL of distilled water, to which was added 300 μL of n-butanol. Then the mixture was vigorously stirred at room temperature, to which was then added 50 μL DMF solution of ZnPc$(OAr)_4$. Then a proper amount of TEVS (100 μL, 125 μL, or 150 μL) was added dropwise within 30 min, and the resulting solution was magnetically stirred for 1 h, after which 10 μL ammonia solution was added. In the end, 15 μL of APTES was added and the final solution was stirred for about 20 h. After the formation of desired nanoparticles, Tween-80 and other unreacted starting materials were removed by vacuum filtration through a 0.45 μm cutoff filter membrane. To completely separate Tween-80 from the nanoparticles, and to purify and concentrate the solution, the filtrated solution was then centrifuged at 13,000 rpm for 30 min. The centrifuged nanoparticles were then washed by distilled water more than 3 times and used for further experimentation.

2.3. Detection of the resultant nanoparticles

Transmission electron microscope (TEM) images were collected using a TECNAI F-30 (Philips-FEI, Netherlands). UV–vis absorption spectra were obtained on a Cary 50 Bio UV–visible spectrophotometer (Varian).

2.4. CL assay

Photoinduced chemiluminescence (PCL) was measured on a BPCL ultra-weak CL analyzer controlled by a personal computer with BPCL program (Institute of Biophysics, Chinese Academy of Sciences). Reactions were initiated by an infrared heat lamp which emitted considerable infrared radiation via a glass filter. The intensity of light was measured with a digital light meter (TES Electrical Electronic Corp.), during which that of the infrared heat lamp was maintained constant. The light level was $17{,}000.0 \pm 15.1$ Lux$=1$ lumen per square meter). Reactions were carried out in a 10 mL quartz cell. All experiments were conducted at room temperature. Temperature of the solution, which was typically increased by ca. 0.5 °C during irradiation, was relatively unimportant.

2.5. Sample preparation

MCLA (5.5×10^{-4} mol/L) and ZnPc$(OAr)_4$ solutions (2.0×10^{-2} mol/L) were respectively dissolved by distilled water and DMF, and then stored in dark until synthesis. The CL reaction mixture producing CL signal consisted of 2.5×10^{-6} mol/L MCLA and ZnPc$(OAr)_4$@SiO_2 ($C = 1.3 \times 10^{-6}$ mol/L) in PBS (pH$=7.4$).

3. Results and discussion

3.1. Characterizations of ZnPc$(OAr)_4$@SiO_2 nanoparticles by TEM and UV–vis spectroscopy

TEM images of the ZnPc$(OAr)_4$@SiO_2 nanoparticles are shown in Fig. 2. The particles are spherical and uniformly distributed with the average size of 100 nm. The aggregation of Pc can affect its

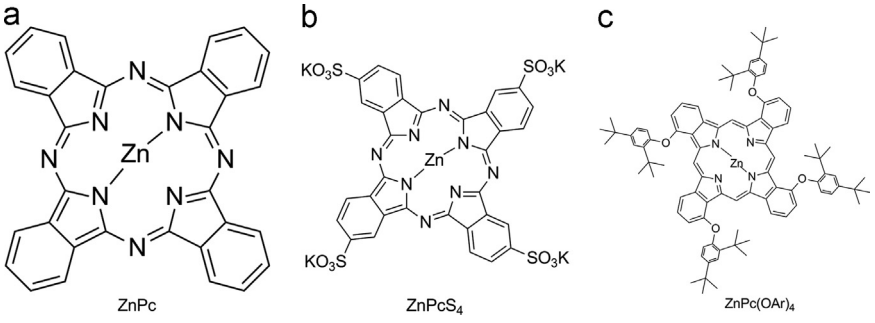

Fig. 1. Chemical structure of ZnPc, $ZnPcS_4$, ZnPc$(OAr)_4$. For the latter two substituted phthalocyanines, which both consist of 4 possible isomers, only one isomer's structure was shown as representive.

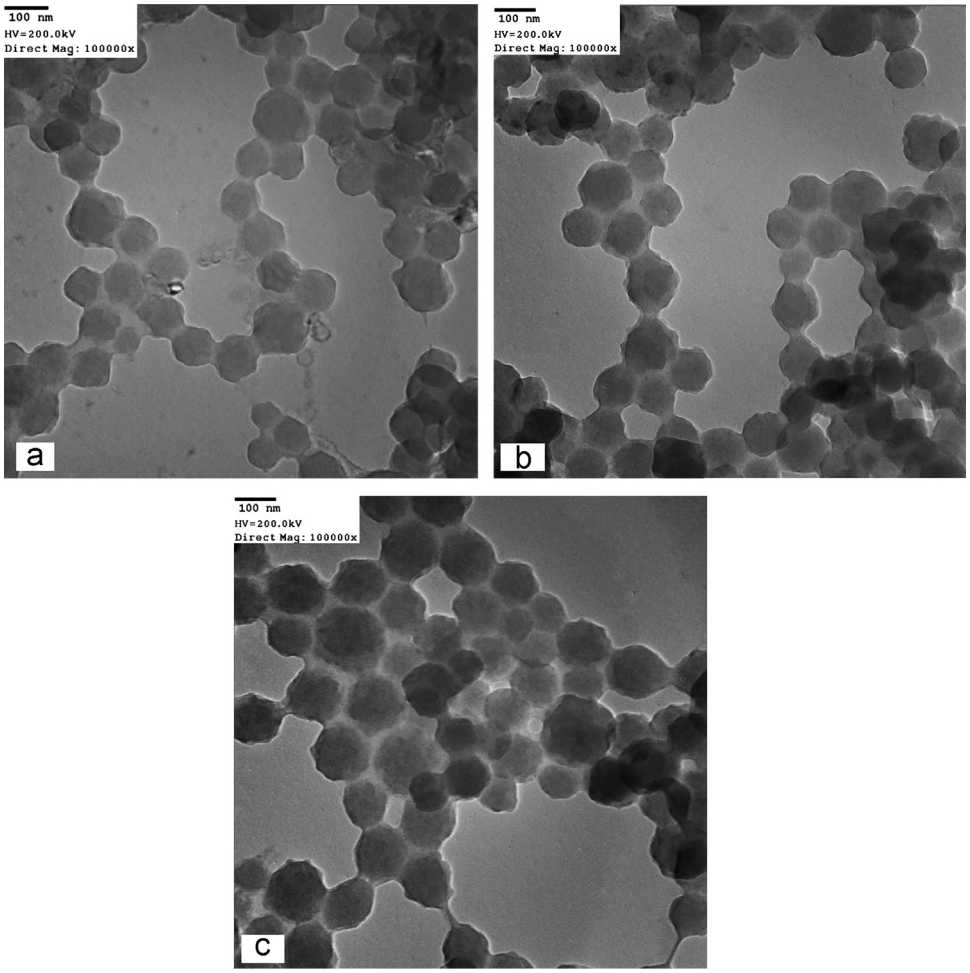

Fig. 2. TEM pictures of $ZnPc(OAr)_4@SiO_2$ nanoparticles showing monodispersed particles with an average diameter of 100 nm. The volume ratio of TEVS added in (a), (b) and (c) is 1.0:1.25:1.5.

photophysical, photochemical and biological properties (Nyokong et al., 1987). In general, the decreasing intensity and hypochromatic shifting of a broadened Q-band absorption is associated with the aggregation of phthalocyanine molecules in aqueous solution. Hence, the Q-band absorptions of $ZnPc(OAr)_4$ were studied under different conditions to estimate the aggregation extents.

Phthalocyanines with bulky and rigid substituents on the alfa-position are prone to dissolution with low tendency of aggregation in common organic solvents such as DMF because of steric crowding effect (George et al., 1998; Jiang et al., 2005). It is also the case for $ZnPc(OAr)_4$. The Q-band absorptions of free $ZnPc(OAr)_4$ and $ZnPc(OAr)_4@SiO_2$ nanoparticles in DMF almost resemble. The sharp peaks centered at 701 nm represent the phthalocyanine molecules are monomers (Fig. 3). Free $ZnPc(OAr)_4$ is barely soluble in water and precipitates from the solution even adding DMF (about 1:3, v/v), thus rendering UV–vis spectroscopy ineffective. In contrast, when encapsulated in SiO_2 nanoparticles, $ZnPc(OAr)_4$ can form a stable dispersion in aqueous solution. Although compared to that in DMF, the Q-Band absorption peak of ZnPc(OAr)4@SiO2 in water is broader and weaker with a slight bathochromic shift, which indicates the existence of mild J-aggregation, the monomeric state is predominant. The non-aggregation property is mainly attributed to the steric crowding effect of the bulky substituents on the non-peripheral positions of the phthalocyanine ring, which prevents a second phthalocyanine molecule form forming a coplanar dimer. The silica nanoparticles improve the aqueous solubility of $ZnPc(OAr)_4$ as carriers.

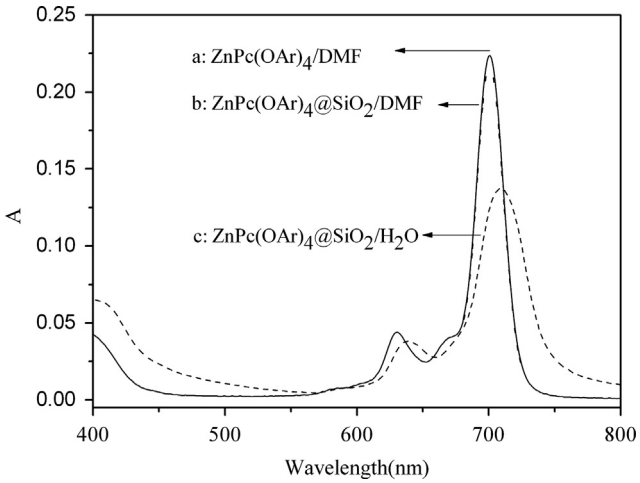

Fig. 3. UV–visible absorption spectra of (a) $ZnPc(OAr)_4$ in DMF, (b) $ZnPc(OAr)_4@SiO_2$ in DMF, (c) $ZnPc(OAr)_4@SiO_2$ in H_2O (the phthalocyanine concentration of three samples is 2.0×10^{-6} mol/L).

In addition, the stability and dispersion of nanomaterials were investigated in PBS buffers at different pH. The results show that pH have no noticeable influence on the nanoparticles. Therefore, the PBS buffer at pH 7.4, which is close to physiological solution, was chosen as the appropriate aqueous solvent for $^1O_2$ detection.

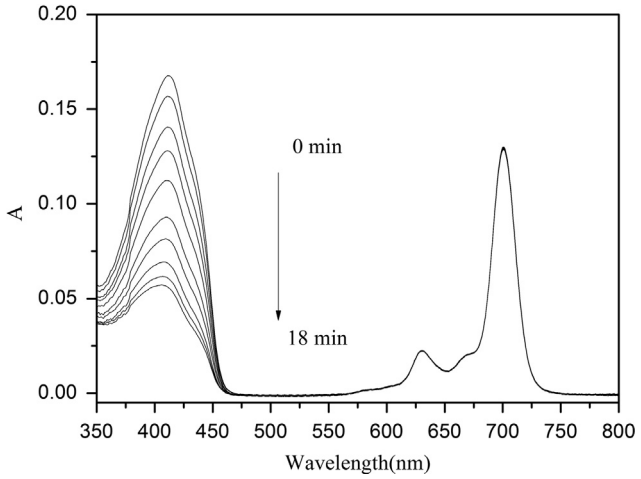

Fig. 4. Photobleaching of DPBF by $ZnPc(OAr)_4$@SiO_2 ($C=1.3\times10^{-6}$ mol/L) in DMF during 701 nm-irradiation. The absorption spectra were recorded each 2 min at room temperature.

3.2. $^1O_2$ quantum yields determination by chemical method

$^1O_2$ generation was estimated using 1,3-diphenylisobenzofuran (DPBF), a well-known $^1O_2$ indicator (Awuah et al., 2011). Nonsubstituted phthalocyanine zinc (ZnPc), whose $^1O_2$ quantum yield is 0.56 in DMF (Ogunsipe and Nyokong, 2005), was used as the reference to those of the nanoparticles. When the mixture of DPBF and $ZnPc(OAr)_4$ was irradiated at 701 nm for over 18 min, the absorption intensity of DPBF decreased dramatically with increasing time, while that of $ZnPc(OAr)_4$ remained nearly unchanged (Fig. 4).

As a control, the UV–vis spectra of the mixture of DPBF and ZnPc were also recorded under irradiation at 670 nm. The decreasing rate of DPBF absorption (k_{DPBF}) depended on the irradiation time interval following the first-order kinetics (Fig. 5) (Xu et al., 2011; Shinohara et al., 2006) (Eq. (1)) (t: irradiation time, A_0: absorbance at $t=0$, A_t: absorbance at different times).

$$\ln(A_0/A_t) = k_{DPBF} \times t \quad (1)$$

The absorption rate of photons by PS (k_{pho}) under irradiation was calculated by Eq. (2) (P: the irradiating laser power (mW), A: absorbance, per cm, of the sensitizer at λ, λ: irradiation wavelength (nm), L: light path length of beam (cm), V: sample volume (ml), 0.97: correction coefficient of reflected light from laser in air and on glass contact surface, $0.1197/\lambda$: energy of 1 mol photon).

$$k_{pho} = \frac{0.97 \times P \times (1-10^{-A\times L})}{(0.1197/\lambda)\times V} \quad (2)$$

$^1O_2$ quantum yields Φ_Δ are proportional to the ratio of the rate of the target's disappearance to the rate of absorption of photons by the sensitizer, k_{DPBF} to k_{pho} (k_{DPBF}/k_{pho}). Given that $\Phi_{\Delta,\ ZnPc}$ is known, $\Phi_{\Delta,\ ZnPc(OAr)\ 4}$ can be calculated from Eq. (3), and $\Phi_{\Delta,\ ZnPc(OAr)\ 4@Sio_2}$ can also be obtained with the same method.

$$\frac{\Phi_{\Delta,\ ZnPc(OAr)\ 4}}{\Phi_{\Delta,\ ZnPc}} = \frac{k_{DPBF,ZnPc(OAr)_4}/k_{pho,ZnPc(OAr)_4}}{k_{DPBF,ZnPc}/k_{pho,ZnPc}} \quad (3)$$

As shown in Fig. 4, the absorption intensity of DPBF at 413 nm reduces over time. Thus, the relationship between $\ln(A_0/A_t)$ and time was plotted (Fig. 5a). The slope $k_{DPBF,\ ZnPc(OAr)\ 4}$ derived from linear fitting is $6.197\times10^{-4}\ s^{-1}$. The negligible decay of blank contrast sample of DPBF without PS excludes the influence of self-oxidation, based on which $\Phi_{\Delta,\ ZnPc(OAr)\ 4}$ was calculated as 0.70 by Eq. (2) and Eq. (3). Likewise, $\Phi_{\Delta,\ ZnPc(OAr)\ 4@Sio_2}$ was calculated as 0.68(Fig. 5b). The results suggest that silica nanoparticles do not affect the photodynamic activity of the phthalocyanine embedded.

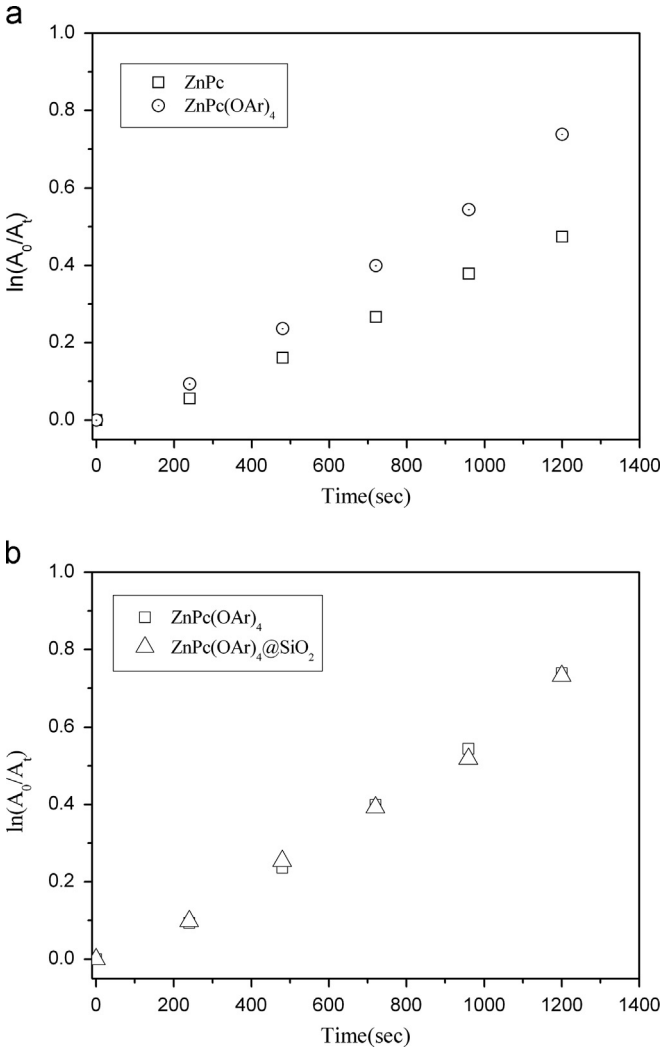

Fig. 5. Plots of $\ln(A_0/A_t)\sim t$ for the photobleaching of DPBF by ZnPc ($\lambda=670$ nm), $ZnPc(OAr)_4$ ($\lambda=701$ nm) and $ZnPc(OAr)_4$@SiO_2 ($\lambda=701$ nm) under the same phthalocyanine concentration, 1.3×10^{-6} mol/L.

3.3. $^1O_2$ detection in aqueous solution by CL method

Previously, we have detected $^1O_2$ in aqueous solution by CL method with MCLA as the luminous agent (Wang et al., 2006), which proved that phthalocyanines were sufficiently efficient to initiate the luminescence of MCLA under red light irradiation, corresponding to the Q-band absorption of the dyes. Singlet oxygen ($^1O_2$) has a lifetime highly dependent on the medium, which ranges from 10–100 ms in organic solvents and approximately 2 μs in water (Macdonald and Dougherty, 2001). So $^1O_2$ can diffuse a certain distance, such as 10 nm from where it is produced. Thus it can pass the mesoporous silica shell and participate in chemiluminescence reactions in solution.

A water-soluble phthalocyanine, $ZnPcS_4$, with the $^1O_2$ quantum yield of 0.52 in DMF (Ogunsipe and Nyokong (2005)), was used as the reference. The absorption intensities of $ZnPc(OAr)_4$@SiO_2 and $ZnPcS_4$ solutions dissolved in PBS buffer (pH=7.4) were identical. In the beginning, 0.5 μL of MCLA was quickly mixed with 200 μL of sample solution. Promptly, the mixture solution was irradiated for some seconds at appropriate wavelength (the absorption maxima

of $ZnPc(OAr)_4$ and $ZnPcS_4$ were 701 nm and 635 nm). The delayed CL signal intensities at variable time points were recorded on the BPCL ultra-weak CL analyzer.

Fig. 6 exhibits the decay curve of CL intensity after the solutions were irradiated. Compared with PBS in the same condition, both $ZnPcS_4$ and $ZnPc(OAr)_4@SiO_2$ induced intense CL of MCLA. Meanwhile, the signal induced by $ZnPc(OAr)_4@SiO_2$ was stronger than that by $ZnPcS_4$, indicating $ZnPc(OAr)_4@SiO_2$ may generate $^1O_2$ more effectively than $ZnPcS_4$.

3.4. PCL response characteristics of the aptamer/thrombin/aptamer sensor

The PCL responses of the target protein thrombin were detected. Thrombin was selected as the target analyte to experimentally validate the sandwich assay based on ELISA principle, which involved two thrombin-binding aptamers (THR-1 and THR-2) recognizing two different epitopes of the protein (Scheme 1). Thrombin is selectively captured on the aptamer (THR-1)-modified magnetic beads and the $ZnPc(OAr)_4@SiO_2$ labeled secondary aptamer (THR-2).

The UV–vis absorption peak intensity of $ZnPc(OAr)_4$ (Fig. 7a) was proportional to the amount of human thrombin. Thrombin was also measured by PCL, as shown in Fig. 7b. When the blank buffer was added, the PCL signal did not increase apparently, while it rose accordingly with elevating concentration of the target protein. During the experiment, the CL signal did not increase apparently, while its PCL intensity was enhanced with increasing amount of thrombin. The decays of PCL intensity (Fig. 7b) can be better described by two-exponential fittings as: $y=y_0+A_1\times\exp(-(x-x_0)/t_1)+A_2\times\exp(-(x-x_0)/t_2)$, where y is the variable CL intensity, y_0 is the basic CL intensity, A_1 and A_2 are the amplitudes and t_1 and t_2 are the time constants. The two-exponential functions can be used to predict the maximum initial PCL emission intensity.

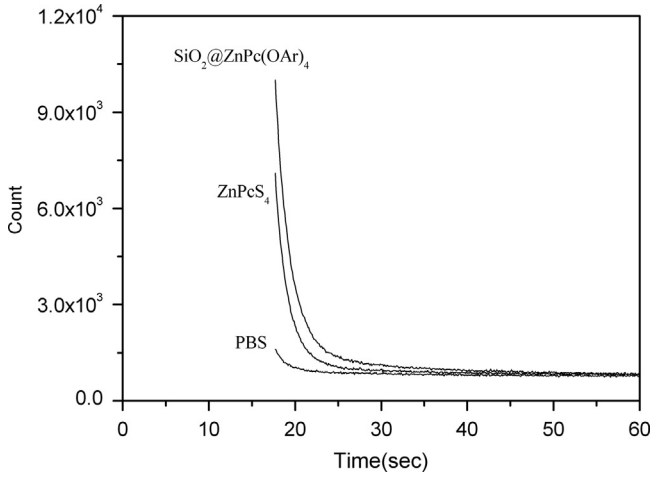

Fig. 6. The delayed CL curves of MCLA after being irradiated for 15 s. (a) 1.3×10^{-6} mol/L $ZnPc(OAr)_4@SiO_2$ at 701 nm, (b) 1.3×10^{-6} mol/L $ZnPcS_4$ at 635 nm and (c) PBS (pH=7.4) at 701 nm.

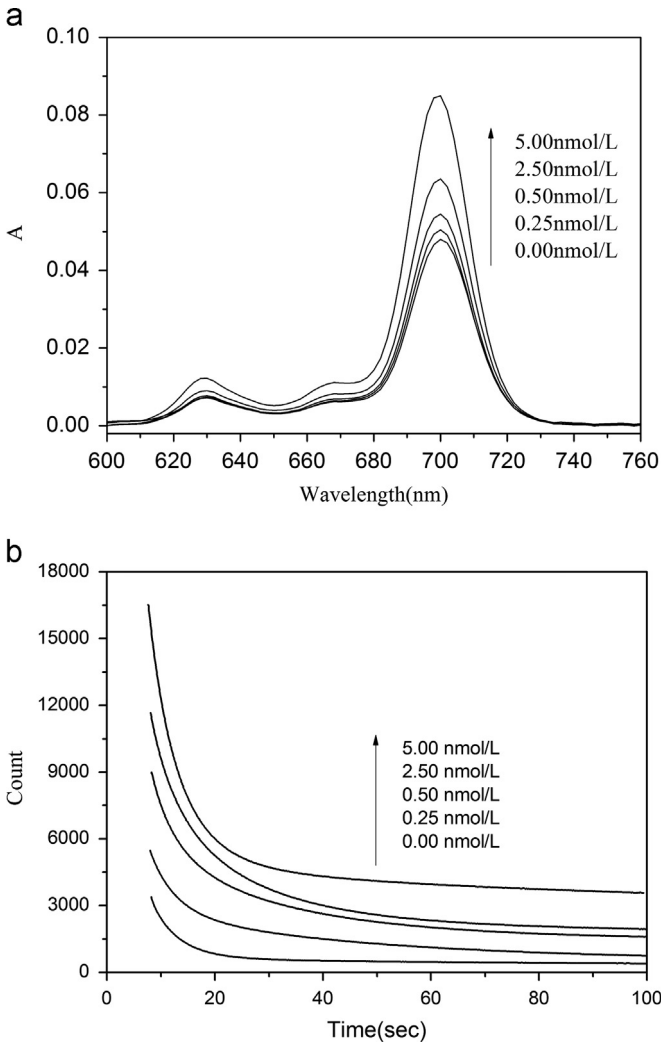

Fig. 7. Spectra of thrombin (from 0.00 nmol/L to 5.00 nmol/L) and $ZnPc(OAr)_4@SiO_2$ ($ZnPc(OAr)_4$ concentration is 1.3×10^{-6} mol/L) with PBS (pH=7.4) as reference. (a) UV–vis absorption spectra and (b) The delayed CL curves after irradiating for 8 s at 701 nm.

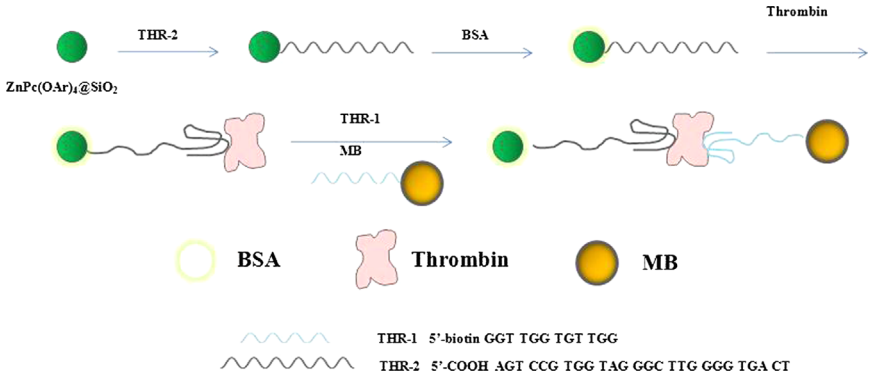

Scheme 1. Schematic diagram shows the principle of the aptamer-capture for human thrombin.

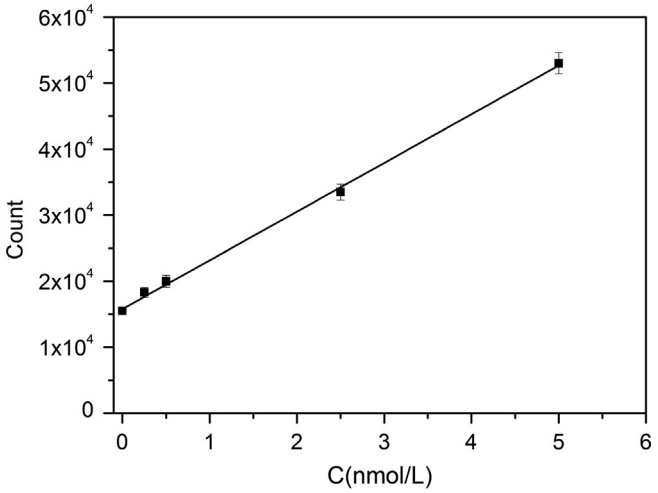

Fig. 8. The fitting curve of initial CL intensity ($t=0$) for detecting thrombin by ZnPc $(OAr)_4$@SiO_2 (the phthalocyanine concentration is 1.3×10^{-6} mol/L).

3.5. Method validation: linearity and limit of quantification

Correlation between the concentration of thrombin and the initial PCL intensity (when t=0), i.e. $I=7.34\times10^3$ c/nmol/L+ 1.59×10^4, was plotted. The PCL of different concentrations of thrombin are shown in Fig. 8. The concentrations of thrombin ranging from 250 pmol/L to 5 nmol/L were suitable for quantitatively analyzing low-level proteins. In case thrombin was excess, the reduced aptamer-thrombin binding capacity raised the PCL signal slowly. The resulting regression coefficient (or correlation coefficient) of the calibration curve was 0.996. The limit of detection (LOD, $S/N=3$) of thrombin was 80 pmol/L (RSD=9.3%), being lower than those reported in a previous literature (100 pmol/L −2.8 nmol/L) (Numnuam et al., 2008).

The intra-assay precision and accuracy of the method was determined from the results of the samples prepared in triplicate at three concentrations on 2 separate days. The precisions of the method for the determination of thrombin are also summarized in Table 1. Intra-day precision ranged from 6.1% to 9.6%, and inter-day precision ranged from 8.2% to 12.2%. The results demonstrate the efficiency of the method with little variation.

4. Conclusions

New silica nanoparticles embedded with a hydrophobic Pc were synthesized to develop PSs with high $^1O_2$ generation efficiency in aqueous solution. The doped particles were uniformly size-distributed with the average diameter of 100 nm, and were formulated as a stable aqueous dispersion. Although phthalocyanine was embedded in the silica particle matrix, it was still excited by irradiation at appropriate wavelength to produce $^1O_2$ effectively as a prerequisite for PDT activity. The $^1O_2$ production suggests that ZnPc$(OAr)_4$@SiO_2 is potentially applicable in PDT. Further studies, such as surface modification of silica-based particles, will guide our ongoing development of PSs. A sensitive aptamer-based sandwich-type sensor by using ZnPc$(OAr)_4$@SiO_2 as the PCL label was developed to detect as low as 80 pmol/L thrombin in human serum. This method is promising in detecting and screening ultratrace levels of biomarkers in complex matrices.

Table 1
Recovery for determination of thrombin.

Spiked concentration (nmol/L)	Intrarun precision ($n=3$)		Interrun precision ($n=6$)	
	Average recovery (%)	CV (%)	Average recovery (%)	CV (%)
0.25	95.76	9.6	93.32	10.3
1.0	90.83	7.1	90.92	12.2
5.0	84.39	6.2	81.21	8.2

Acknowledgments

This project was supported by the National Natural Sciences Foundation of China. (Grant no. 81273548), the Foundation of the Education Department of Fujian Province, China (JK2010003) and the Scientific and Technological Foundation of Fujian Province of China (2011J01043).

References

Awuah, S.G., Polreis, J., Biradar, V., You, Y., 2011. Org. Lett. 13 (15), 3884–3887.
Bechet, D., Couleaud, P., Frochot, C., Viriot, M.L., Guillemin, F., Barberi-Heyob, M., 2008. Trends Biotechnol. 26 (11), 612–621.
Bock, L.C., Griffin, L.C., Latham, J.A., Vermaas, E.H., Toole, J.J., 1992. Nature 355 (6360), 564–566.
Cho, H., Baker, B.R., Wachsmann-Hogiu, S., Pagba, C.V., Laurence, T.A., Lane, S.M., Lee, L.P., Tok, J.B.H., 2008. Nano Lett. 8 (12), 4386–4390.
Dolmans, D.E., Fukumura, D., Jain, R.K., 2003. Nat. Rev. Cancer 3 (5), 380–387.
George, R.D., Snow, A.W., Shirk, J.S., Barger, W.R., 1998. J. Porphyr. Phthalocya. 2 (1), 1–7.
Huang, Z., 2005. Technol. Cancer Res. T 4 (3), 283–293.
Jiang, Z., Chen, N.S., Wang, J.D., Huang, J.L., 2005. Chin. J. Inorg. Chem. 21 (12), 1891–1896.
Kim, S., Ohulchanskyy, T.Y., Bharali, D., Chen, Y., Pandey, R.K., Prasad, P.N., 2009. J. Phys. Chem. C 113 (29), 12641–12644.
Leznoff, C.C., Lever, A.B.P., 1989–1996. Phthalocyanines Properties and Applications. vol. 1–4. VCH, Weinheim.
Macdonald, I.J., Dougherty, T.J., 2001. J. Porphyr. Phthalocya. 5 (2), 105–129.
Niu, Y.J., Wang, P., Zhao, Y.J., Fan, A.P., 2013. Analyst 138 (5), 1475–1482.
Numnuam, A., Chumbimuni-Torres, K.Y., Xiang, Y., Bash, R., Thavarungkul, P., Kanatharana, P., Pretsch, E., Wang, J., Bakker, E., 2008. Anal. Chem. 80 (3), 707–712.
Nyokong, T., Gasyna, Z., Stillman, M.J., 1987. Inorg. Chem. 26 (7), 1087–1095.
Ogunsipe, A., Nyokong, T., 2005. J. Photoch. Photobio. A 173 (2), 211–220.
Rossi, L.M., Shi, L.F., Quina, F.H., Rosenzweig, Z., 2005. Langmuir 21 (10), 4277–4280.
Roy, I., Ohulchanskyy, T.Y., Pudavar, H.E., Bergey, E.J., Oseroff, A.R., Morgan, J., Dougherty, T.J., Prasad, P.N., 2003. J. Am. Chem. Soc. 125 (26), 7860–7865.
Sadzuka, Y., Iwasaki, F., Sugiyama, I., Horiuchi, K., Hirano, T., Ozawa, H., Kanayama, N., Sonobe, T., 2007. Int. J. Pharm. 338 (1–2), 306–309.
Shinohara, H., Tsaryova, O., Schnurpfeil, G., Wohrle, D., 2006. J. Photochem. Photobiol. A 184 (1–2), 50–57.
Tang, W., Xu, H., Kopelman, R., Philbert, M.A., 2005. Photochem. Photobiol. 81 (2), 242–249.
Triesscheijn, M., Baas, P., Schellens, J.H., Stewart, F.A., 2006. Oncologist 11 (9), 1034–1044.
Wang, J., Jiang, Z., Chen, N.S., Huang, J.L., 2006. Microchim. Acta 153 (1–2), 79–85.
Wang, S.Z., Gao, R.M., Zhou, F.M., Selke, M., 2004. J. Mater. Chem. 14 (4), 487–493.
Xu, H., Gorgy, K., Gondran, C., Goff, A.L., Spinelli, N., Lopez, C., Defrancq, E., 2013. Biosens. Bioelectron. 41, 90–95.
Xu, X.Z., Wang, J., Li, Z.L., Yan, W.J., Chi, H.L., Chen, W.B., Zhuo, S.C., Chen, N.S., 2011. Chin. J. Inorg. Chem. 27 (5), 877–885.
Yan, F., Kopelman, R., 2003. Photochem. Photobiol. 78 (6), 587–591.
Yang, H., Ji, J., Liu, Y., Kong, J.L., Liu, B.H., 2009. Electrochem. Commun. 11 (1), 38–40.
Zhu, J., Wang, H., Liao, L., Zhao, L., Zhou, L., Yu, M., Wang, Y., Liu, B., Yu, C., 2011. Chem.-Asian J. 6 (9), 2332–2338.